ECS Transactions, 33 (5) 345-353 (2010)
10.1149/1.3481257 ©The Electrochemical Society

# Characteristics of Zinc Oxide Thin Film Transistors Fabricated by Location-Controlled Hydrothermal Method

P. Y. Yang[a*], J. L. Wang[b], W. C. Tsai[c], S. J. Wang[c], P. C. Chen[d], N. C. Su[c], J. C. Lin[e], I. C. Lee[a], C. T. Chang[a], Y. C. Wei[a], and H. C. Cheng[a]

[a] Department of Electronics Engineering and Institute of Electronics, National Chiao Tung University, Hsinchu 30010, Taiwan
[b] Department of Electronics Engineering, Ming Chi University of Technology, Taipei 24301, Taiwan
[c] Institute of Microelectronics, Department of Electrical Engineering, National Cheng Kung University, Tainan 70101, Taiwan
[d] Department of Materials and Engineering, National Chiao Tung University, Hsinchu 30010, Taiwan
[e] Department of Electronics Engineering, St. John's University, Taipei 25135, Taiwan

In this paper, high-performance Zinc oxide (ZnO) thin-film transistors (TFTs) with bottom-gate (BG) structure and artificially location-controlled lateral grain growth have been prepared by low-temperature hydrothermal method. As the proper design of source/drain structure of ZnO/Ti/Pt thin films, the lateral grain growth can be artificially controlled in the desired location and the vertical grain boundary perpendicular to the current flow in the channel region can be reduced to single one. As compared with the conventional sputtered ZnO BG-TFTs, the proposed location-controlled hydrothermal ZnO BG-TFTs (W/L = 250 μm/10 μm) demonstrated the higher field-effect mobility of 6.09 $cm^2/V\cdot s$, lower threshold voltage of 3.67 V, larger on/off current ratio above $10^6$, and superior current drivability, which can be attributed to the high-quality ZnO thin films with the reduced vertical grain boundaries in the channel region.

## Introduction

Zinc oxide (ZnO) is an n-type II–VI compound semiconductor, and it possesses a direct energy wide-bandgap (i.e. ~3.37 eV) at room temperature, a large exciton binding energy (i.e. ~60 meV), good photoelectric and piezoelectric properties, and high optical transparency for visible light (1). Therefore, ZnO has been investigated for various applications including ultraviolet photodetector (2), gas sensors (3), solar cells (4), light emitting diodes (LED) (5), and transparent electrodes (6), surface acoustic wave devices (SAW) (7). Recently, ZnO as an active channel layer has been investigated for transparent thin film transistor (TFT) (8)-(10) and compared with amorphous silicon TFTs (11)-(12) and organic TFTs (13)-(15). Essentially, the organic TFTs may degrade in atmospheric conditions (16)-(17) and amorphous silicon TFTs have been presented for some limitations of optical applications, such as light sensitivity, light degradation and opaqueness (18). On the contrary, ZnO TFTs disclose not only the high transparency within the visible-light spectra but also the relatively high field effect mobility, less light


Downloaded on 2014-04-24 to IP 140.113.38.11 address. Redistribution subject to ECS terms of use (see ecsdl.org/site/terms_use) unless CC License in place (see abstract).

sensitivity, and excellent chemical and thermal stability (19), indicating the potentials of ZnO-based thin films applied in TFTs. The ZnO-based thin films have been prepared by various vacuum-based deposition techniques, such as pulsed laser deposition (PLD) (8), and sputtering (9), atomic layer deposition (10), and chemical vapor deposition (CVD) (20), which usually suffer the issues of expensive facilities, low throughput, complicated operating conditions and high energy consumption. In contrast, solution-based deposition processes, i.e. sol-gel process (21), chemical bath deposition (CBD) (22), and aqueous solution-growth method (23) offer a comparatively simple, low cost, and large area thin-film coating deposition techniques. Furthermore, a large number of grain boundaries can be observed due to the small grains of ZnO film formed polycrystalline phase easily at room temperatures (24)-(26). The localized potential barriers of grain boundaries are produced to retard the passage of carrier from grain to grain (27). The presence of grain boundaries in the channel region of poly-ZnO TFT's has a dramatic influence on the electrical characteristics. Hence, enlarging grain size can be a greatly effective method for improving device performances. For the realizing of high-performance ZnO TFTs, it is essential not only to require larger ZnO grains but also to control the locations, number and direction of grain boundaries in ZnO active layer.

In this work, a simple hydrothermal method was adopted for ZnO thin films growth because of the advantages of low-cost facility, capabilities of large-area and uniform fabrication, and environmental friendliness. Moreover, the grain size and direction of grain boundaries in ZnO active layer were designed with the technique of location-controlled nucleation at the selected region, and the related devices performances of ZnO TFTs are also addressed.

## Experimental Procedure

Figure 1 illustrates the key processes for the fabrication of hydrothermally grown ZnO bottom-gate-TFTs (BG-TFTs) with the technique of location-controlled nucleation. A 200 nm sputtered indium-tin-oxide (ITO) film was used as the gate electrode on the glass substrate. After cleaning, a 200 nm-thick tetraethylorthosilicate silicon dioxide (TEOS-$SiO_2$) layer was deposited as gate dielectric by plasma-enhanced chemical vapor deposition (PECVD) at 350 °C. Next, a ZnO film (~200 nm) and Ti (~100 nm)/Pt (~50 nm) films were deposited on $SiO_2$/ITO glass substrate by using a sputtering system at room temperature. The ZnO and Ti/Pt films were patterned by a lifting-off technique and acted as a seed layer and contact metal, correspondingly. The samples were dipped in 0.001 M $H_3PO_4$ and then immersed in the mixed hydrothermal growth solution. The growth solution was prepared by mixing with 0.25 M zinc nitrate hexahydrate ($Zn(NO_3)_2 \cdot 6H_2O$) and 0.25 M hexamethylenetetramine (HMTA) in deionized water at 85 °C for 180 minutes. Subsequently, the samples were thoroughly rinsed with deionized water in order to eliminate residual salts and dried in air at room temperature. Finally, the samples were annealed at 400 °C for one hour in $O_2$ ambience. For comparison, a conventional sputtered ZnO BG-TFTs with a channel thickness of 200 nm were fabricated and measured. After TFTs formation, an automatic measurement system that combines IBM PC/AT, semiconductor parameter analyzer (4156C, Agilent Technologies) and a probe station were used to measure the I–V characteristics. The surface morphologies were observed by a field-emission scanning electron microscopy (FE-SEM, Hitachi S-4700I). An analytical field-emission transmission electron microscopy (JEM-2100FX, JEOL Ltd.) was employed to analyze the microstructure and



Downloaded on 2014-04-24 to IP 140.113.38.11 address. Redistribution subject to ECS terms of use (see ecsdl.org/site/terms_use) unless CC License in place (see abstract).

crystallinity of the ZnO thin films in the channel region of BG ZnO TFTs. The samples of cross-section TEM were prepared by focused-ion-beam (FIB) technique (Nova 200, FEI Company).

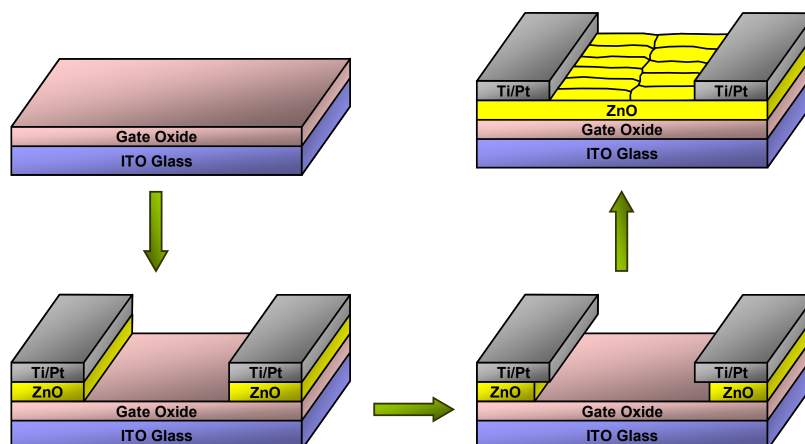


**Figure 1.** The key processes for fabricating location-controlled hydrothermal ZnO BG-TFTs.

## Results and Discussion

The field-emission scanning electron microscopy (FE-SEM) image (45° tilt view) of ZnO film sputtered on gate oxide at room temperature is shown in Figure 2(a). It is observed that the thickness of ZnO thin film is about 200 nm and the film exhibits a densely polycrystalline microstructure. The inset of Figure 2(a) shows an optical micrograph of the conventional sputtered ZnO BG-TFTs with the channel length of 10 μm. The FE-SEM image of location-controlled hydrothermal ZnO BG-TFTs is shown in Figure 2(b), which confirms that the ZnO grain growth only existed between the electrodes of sputtered Ti/Pt and no ZnO thin films are watched on the electrodes. The lateral grain growth started from the edges of ZnO seed layer underlying the Ti/Pt films, and extended toward the middle of channel from opposite direction impinges. It is seen that the achievable length of lateral grain growth using this hydrothermal method is about 5 μm while the distance between source and drain is 10 μm. The inset of Figure 2(b) presents the enlarged image of the device channel, revealing that the grain boundaries located at the middle of channel where grains collided due to the grain growth from opposite direction. The micro-structural properties of location-controlled hydrothermal ZnO BG-TFTs can be identified by using TEM and its selected-area electron diffraction (SAED) patterns. Figure 2(c) displays the cross-sectional TEM image and the SAED patterns of 200 nm-thick ZnO thin films with BG structure after hydrothermal growth. There are two large ZnO grains formed in the channel region above the BG electrode and the vertical grain boundary can be artificially controlled in the middle of the channel region, which is consistent with the observation of Fig. 2(b). According to the TEM image, the location-controlled lateral grain growth collided at the middle of channel, resulting in only single grain boundary perpendicular to the channel direction and the rugged morphology of hydrothermal ZnO films. The crystallinity of the ZnO grains in the channel region is single-crystalline wurtzite structure based on the simple spots in the inserted SAED patterns. Moreover, the orientation of grain growth is



Downloaded on 2014-04-24 to IP 140.113.38.11 address. Redistribution subject to ECS terms of use (see ecsdl.org/site/terms_use) unless CC License in place (see abstract).

along the [0001] direction, the *c*-axis of ZnO crystal, which is the fastest growth direction for ZnO crystals.

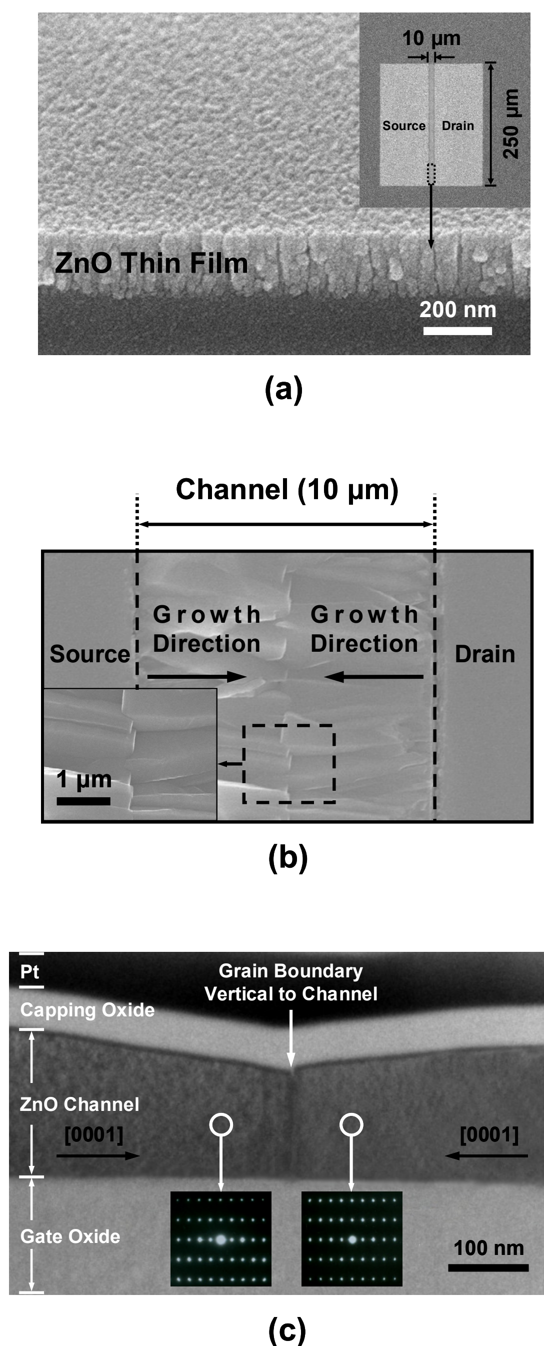


**Figure 2.** (a) The FE-SEM image (45° tilt view) of ZnO film sputtered on gate oxide at room temperature. An optical micrograph of the conventional sputtered ZnO BG-TFTs is shown in the inset. (b) The FE-SEM images of location-controlled hydrothermal ZnO BG-TFTs, where the channel length is 10 μm. The inset shows the enlarged device-channel image of location-controlled hydrothermal ZnO BG-TFTs structure. (c) The cross-sectional TEM image and SAED patterns of location-controlled hydrothermal ZnO BG-TFTs.



Downloaded on 2014-04-24 to IP 140.113.38.11 address. Redistribution subject to ECS terms of use (see ecsdl.org/site/terms_use) unless CC License in place (see abstract).

Figure 3 gives a schematic illustration for the hydrothermally lateral grain growth of ZnO BG-TFTs. As the proper design of source/drain structure of ZnO/Ti/Pt thin films, the lateral grain growth can be artificially controlled in the desired location and the vertical grain boundary perpendicular to the current flow in the channel region can be reduced to single one. The reduced vertical grain boundary in channel region is expected to produce the better device performance of ZnO BG-TFTs.

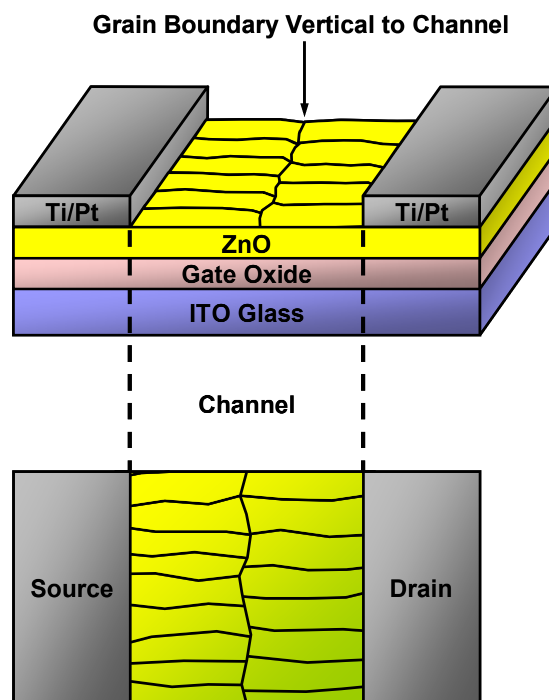


**Figure 3.** The schematic illustration of lateral grain growth in location-controlled hydrothermal ZnO BG-TFTs. A single grain-boundary vertical to channel can be observed in this scheme.

To evaluate the devices performances and electrical characteristics of location-controlled hydrothermal ZnO BG-TFTs, the conventional sputtered ZnO BG-TFTs with a thickness of 200 nm were also fabricated and measured for comparison. Figure 4 depicts the drain-current–gate-voltage (the plots of $I_{DS}$–$V_{GS}$ and $I_{DS}^{1/2}$–$V_{GS}$) transfer characteristics for location-controlled hydrothermal and conventional sputtered ZnO BG-TFTs with channel width ($W$) of 250 μm and channel length ($L$) of 10 μm at drain voltage ($V_{DS}$) of 20 V. The threshold voltage ($V_{TH}$) and field-effect mobility ($\mu$) were defined by fitting a straight line to the plot of the square root of drain current versus gate voltage, calculated by the formula of saturated regions:

$$I_{DS,SAT} = \frac{\mu W C_{OX}}{2L}(V_{GS} - V_{TH})^2 \qquad [1]$$

where $I_{DS,SAT}$ is the saturated drain current, and $C_{OX}$ is the capacitance per unit area of gate insulator, respectively. The location-controlled hydrothermal ZnO BG-TFTs

Downloaded on 2014-04-24 to IP 140.113.38.11 address. Redistribution subject to ECS terms of use (see ecsdl.org/site/terms_use) unless CC License in place (see abstract).

demonstrates the threshold voltage of 3.67 V and field effect mobility of 6.09 $cm^2/V{\cdot}s$. On the contrast, the threshold voltage and mobility of conventional sputtered ZnO BG-TFTs are about 7.02 V and 2.25 $cm^2/V{\cdot}s$, accordingly. Both kinds of TFTs require positive gate voltage to turn-on, suggesting the behaviours of n-channel device and enhancement-mode. Table 1 summarizes the electrical characteristics of these two different TFT devices. The superior device performances (i.e. the higher mobility, lower threshold voltage, larger on/off current ratio, and excellent current drivability) can be evidently obtained in location-controlled hydrothermal ZnO BG-TFTs, which can be attributed to the high-quality ZnO thin films with the reduced vertical grain boundaries in the channel region. It is well known that the grain boundary acts as a strong trapping center which degrades the performance of TFTs, resulting in an increase in threshold voltage, a decrease in mobility, a raise in leakage current, and worse device stability (28). The higher threshold voltage and lower mobility present the more defects in channel region, which require the larger gate voltage in order to fill the great number of trap states before the device can turn on. On the other hand, after trapping the free carriers in the grain boundaries, the defect states become electrically charged and created a potential energy barrier, which act as potential barriers during carrier transport from drain to source (28).

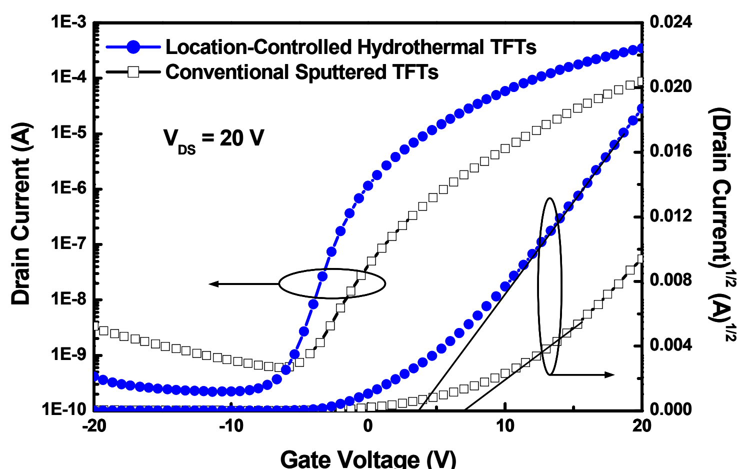


**Figure 4.** The drain-current–gate-voltage ($I_{DS}$, $I_{DS}^{1/2}$–$V_{GS}$, at constant $V_{DS}$ = 20 V) transfer characteristics for location-controlled hydrothermal ZnO BG-TFTs and conventional sputtered ZnO BG-TFTs.

**TABLE I.** Measured electrical characteristics of location-controlled hydrothermal ZnO BG-TFTs and conventional sputtered ZnO BG-TFTs.

| | Conventional Sputtered ZnO BG-TFTs | Location-Controlled Hydrothermal ZnO BG-TFTs |
|---|---|---|
| Mobility ($cm^2/V{\cdot}s$) | 2.25 | 6.09 |
| Threshold Voltage (V) | 7.02 | 3.67 |
| ON/OFF Current Ratio | $1.46{\times}10^5$ | $1.58{\times}10^6$ |



Downloaded on 2014-04-24 to IP 140.113.38.11 address. Redistribution subject to ECS terms of use (see ecsdl.org/site/terms_use) unless CC License in place (see abstract).

Figure 5 shows the drain-current–drain-voltage ($I_{DS}$–$V_{DS}$) output characteristics of location-controlled hydrothermal and conventional sputtered ZnO BG-TFTs. It is demonstrates that location-controlled hydrothermal ZnO BG-TFTs exhibit the higher driving current than that of conventional sputtered ZnO BG-TFTs under the same bias condition, which is related to the high field effect mobility. In addition, the current crowding phenomenon is observed at the low-drain voltages in the inset of Fig. 5, which may be caused by the large parasitic resistance between active layer and source- electrode (or drain-electrode) (29). Furthermore, the field effect mobility (i.e. 6.09 $cm^2/V{\cdot}s$) of hydrothermal ZnO BG-TFTs in this work can be comparable to those (i.e. 0.24~1.16 $cm^2/V{\cdot}s$) of the ZnO TFTs prepared by the other solution-based processes in literatures (21)-(23), (30)-(31). The relatively lower field effect mobilities of the reported solution-based ZnO TFTs may be connected to the result of more grain boundaries, poorer crystallinity, and film porosity. This experimental result recommends that the proposed hydrothermally growth ZnO BG-TFTs with location-controlled nucleation can achieve the superior electrical characteristics (i.e. the relatively lower threshold voltage and higher mobility) than those of conventional sputtered and the other reported solution-based ZnO TFTs. It suggests that location-controlled hydrothermal ZnO BG-TFTs have a great potential for the applications of high-performance TFTs, i.e. system-on-panel (SOP).

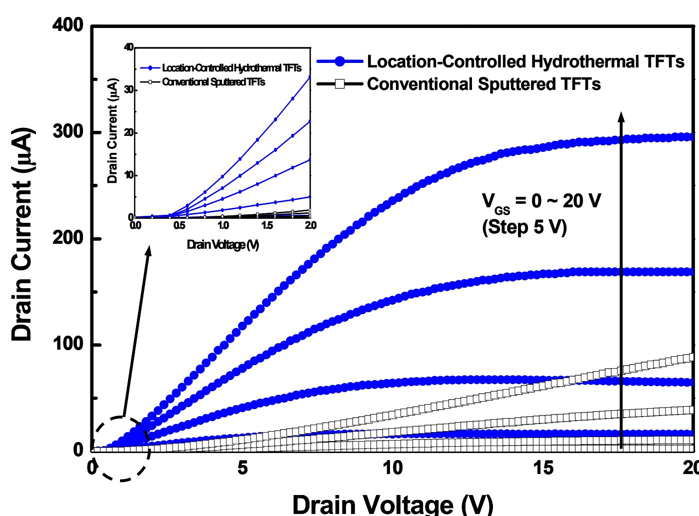


**Figure 5.** The drain-current–drain-voltage ($I_{DS}$–$V_{DS}$) output characteristics for location-controlled hydrothermal ZnO BG-TFTs and conventional sputtered ZnO BG-TFTs. The inset shows the enlarge view of the output characteristics at the low-drain voltages.

## Conclusion

A self-assembled lateral growth ZnO BG-TFT has been fabricated by hydrothermal method on a glass substrate. The lateral grain growth started from the edges of ZnO seed layer underlying the Ti/Pt films, and extended toward the middle of channel from opposite direction impinges. The location-controlled lateral grain growth collided at the middle of channel, resulting in only single grain boundary perpendicular to the channel direction and the rugged morphology of hydrothermal ZnO films. The crystallinity of the ZnO grains in the channel region is single-crystalline wurtzite structure while the


Downloaded on 2014-04-24 to IP 140.113.38.11 address. Redistribution subject to ECS terms of use (see ecsdl.org/site/terms_use) unless CC License in place (see abstract).

orientation of grain growth along the [0001] direction, the *c*-axis of ZnO crystal. The superior device performances (i.e. the higher mobility, lower threshold voltage, and larger on/off current ratio) can be evidently obtained in location-controlled hydrothermal ZnO BG-TFTs, which can be attributed to the high-quality ZnO thin films with the reduced vertical grain boundaries in the channel region. Furthermore, the field effect mobility (i.e. 6.09 $cm^2/V \cdot s$) of hydrothermal ZnO BG-TFTs in this work can be comparable to those (i.e. 0.24~1.16 $cm^2/V \cdot s$) of the ZnO TFTs prepared by the other solution-based processes in literatures. Therefore, the proposed artificially location-controlled hydrothermal ZnO BG-TFTs disclosure the potentials on future active-matrix liquid-crystal display (AMLCD) and high-performance TFTs, i.e. system-on-panel (SOP).

## Acknowledgments

The authors thank the National Science Council of Republic of China for their support under the Contract no. of 98-2218-E-009-004 and 96-2628-E-009-169-MY3. Thanks are also due to the Chung-Shan Institute of Science & Technology, the ChungHwa Picture Tubes, Ltd. (CPT), the Nano Facillity Center (NFC) in National Chiao Tung University, the Chi Mei Optoelectronics, Corp. (CMO), and the National Nano Device Laboratory (NDL) for the technical supports.

## References

1. S. J. Lim, Soonju Kwon, and H. Kim, Thin Solid Films, **516**, 1523 (2008).
2. H. S. Bae and S. Im, *Thin Solid Films*, **469**, 75 (2004).
3. S. P. S. Arya and O. N. Srivastava, *Cryst. Res. Technol.*, **23**, 669 (1988).
4. C. Lee, K. Lim, and J. Song, *Sol. Energy Mater. & Sol. Cells*, **43**, 37 (1996).
5. S. K. Hazra and S. Basu, *Solid State Electron.*, **49**, 1158 (2005).
6. V. Assuncao, E. Fortunato, A. Marques, H. Aguas , I. Ferreira, M. E. V. Coata, and R. Martins, *Thin Solid Films*, **427**, 401 (2003).
7. S. Muthukumar, C. R. Gorla, N. W. Emanetoglu, S. Liang, and Y. Lu, *J. Cryst. Growth*, **225**, 197 (2001).
8. C. J. Kao, Y. W. Kwon, Y. W. Heo, D. P. Norton, S. J. Pearton, F. Ren and G. C. Chi, *J. Vac. Sci. Technol. B.*, **23**, 1024 (2005)
9. P. F. Carcia, R. S. McLean, M. H. Reilly, and G. Nunes, *Appl. Phys. Lett.*, **82**, 1117 (2003).
10. P. F. Carcia, R. S. McLean, and M. H. Reilly, *Appl. Phys. Lett.*, **88**, 123509 (2006).
11. C. R. Kagan and P. Andry, *Thin Film Transistors*, Marcel Dekker, New York (2003).
12. C. S. Yang, L. L. Smith, C. B. Arthur, and G. N. Parsons, *J. Vac. Sci. Technol. B*, **18**, 683 (2000).
13. U. Zschieschang, K. Amsharov, R. T. Weitz, M. Jansen, and H. Klauk, *Synthetic Metals*, **159**, 2362 (2009).
14. A. Facchetti, M. H. Yoon, and T. J. Marks, *J. Am. Chem. Soc.,* **128**, 4928 (2006).
15. M. H. Yoon, A. Facchetti, and T. J. Marks, *Proc. Natl. Acad. Sci.,* **102**, 4678 (2005).
16. Z. Bao, A. J. Lovinger, and J. Brown, *J. Am. Chem. Soc.*, **120**, 207 (1998).
17. H. E. Katz, J. Johnson, A. J. Lovinger, and W. Li, *J. Am. Chem. Soc.*, **122**, 7787 (2000).



Downloaded on 2014-04-24 to IP 140.113.38.11 address. Redistribution subject to ECS terms of use (see ecsdl.org/site/terms_use) unless CC License in place (see abstract).

18. D. L. Staebler, and C. R. Wronski, *Appl. Phys. Lett*., **31**, 291 (1977).
19. C. Y. Tsay, K. S. Fan, S. H. Chen, and C. H. Tsai, *Journal of Alloys and Compounds*, **495**, 126 (2010).
20. Y. Natsume, H. Sakata, and T. Hirayama, *Phys. Status Solidi*, **A 148**, 485 (1995).
21. C. Li, Y. Li, Y. Wu, B. S. Ong, and R. O. Loutfy, *J. Appl. Phys.*, **102**, 076101 (2007).
22. G. A. C. Jones, G. Xiong, and D. Anderson, *J. Vac. Sci. Technol.*, **B 27**, 3164 (2009).
23. H. C. Cheng, C. F. Chen, and C. C. Lee, *Thin Solid Films*, **498**, 142 (2006).
24. S. Masuda, K. Kitamura, Y. Okumura, S. Miyatake, H. Tabata, and T. Kawai, *J. Appl. Phys*., **93**, 3 (2003).
25. Y. Kwon, Y. Li, Y. W. Heo, M. Jones, P. H. Holloway, D. P. Norton, Z. V. Park, and S. Li, *Appl. Phys. Lett*., **84**, 14 (2004).
26. B. J. Norris, J. Anderson, J. F. Wager, and D. A. Keszler, *J. Phys. D: Appl. Phys*., **36**, L105 (2003).
27. F. M. Hossain, J. Nishii, S. Takagi, A. Ohtomo, T. Fukumura, H. Fujioka, H. Ohno, H. Koinuma and M. Kawasaki, *J. Appl. Phys.*, **94**, 7768 (2003).
28. G. Y. Yang, S. H. Hur, and C. H. Han, *IEEE Trans. Electron Devices*, **46**, 165 (1999).
29. J. Nishii, A. Ohtomo, K. Ohtani, H. Ohno and M. Kawasaki, *Jpn. J. Appl. Phys.*, **44**, L1193 (2005).
30. H. C. Cheng, C. F. Chen, and C. Y. Tsay, *Appl. Phys. Lett*., **90**, 012113 (2007).
31. J. Y. Oh, J. Park, S. Y. Kang, C. S. Hwang, and H. K. Shim, *Chem. Commun*., 4545 (2009).




Downloaded on 2014-04-24 to IP 140.113.38.11 address. Redistribution subject to ECS terms of use (see ecsdl.org/site/terms_use) unless CC License in place (see abstract).